Molecular dynamics sampling scheme realizing multiple distributions

Ikuo Fukuda[1] and Haruki Nakamura[1,2]
[1]*National Institute of Advanced Industrial Science and Technology, 2-41-6, Aomi, Koto-ku, Tokyo 135-0064, Japan*
[2]*Institute for Protein Research, Osaka University, 3-2 Yamadaoka, Suita, Osaka 565-0871, Japan*
(Received 12 October 2004; published 25 April 2005)

We present a molecular-dynamics sampling scheme in which any summation of multiple arbitrarily given distributions can be realized deterministically by a certain theoretical guide. Our scheme thus provides a static view of the composition of the distributions, rather than a dynamic view in which some parameter is switched at a certain time in the simulation process. The proposed method induces the orbit to jump automatically among different phase space regions, without the use of any artificial timing parameter. In addition, the proposed method does not require an assumption that the density of states is smooth. We applied it to multiple Tsallis distributions and established a suitable series of parameter values for which the sum of the distributions allows broad sampling. Numerical simulations applied to fundamental models with multi-Tsallis distributions showed efficient sampling, characterized by an energy trajectory that was totally different from that associated with each single distribution.

DOI: 10.1103/PhysRevE.71.046708 PACS number(s): 02.70.Ns, 05.20.Gg, 02.30.Hq, 02.50.Cw

I. INTRODUCTION

For a computer simulation to obtain accurate expected values of objective functions, efficient sampling of states in a given distribution is a crucial task. The Boltzmann-Gibbs (BG) distribution is a typically valuable one in physical issues such as diffusion process in melts [1], glass-forming liquids [2], and structural transitions in biomolecules [3]. To investigate these issues in many realistic continuous systems, molecular dynamics (MD) has provided sampling methods for the BG distribution [4,5]. However, the conventional method has often faced a local trap problem at low temperatures, especially in systems with complicated energy surfaces.

Replica exchange molecular dynamics (REMD) [6,7] and multicanonical molecular dynamics (MCMD) [8–11] have been proven effective at tackling this problem [12]. The REMD produces a product distribution of several BG distributions at distinct temperatures in extended space, exchanging the temperature (or state) for each "replica" according to a certain timing, using appropriate criteria. This process provides a dynamic view in the sense that each "replica" experiences various temperature environments in one simulation. This method has been applied to many problems, including the folding problem in proteins [13,14], and its effectiveness has been demonstrated. Regarding the exchange process characterizing a key feature in the method, it is noticed that the parameter describing this timing as stated above is artificial. A theoretical evaluation of the suitable value of this timing would be desirable because there is a case that the choice of the value has a non-negligible effect on the finite-time simulation results [15]. On the other hand, MCMD provides a static view in which a realization of a certain distribution, defined by a reciprocal of the density of states Ω for the potential energy of a given system, is designed to guide a random walk in the potential energy space. MCMD has been applied extensively, e.g., in studies of peptide secondary structures [16], flexible ligand docking to a receptor [17], protein loop modeling [18], conformational transition states of peptides [19], and force field evaluation [20]. However, determining the distribution weight is not a trivial matter; such determination is often done by using appropriate functions and parameter sets (data) that reflect the required information on Ω. In addition, from a purely mathematical view, it is not generally plausible to assume that the Ω required in the formulation is smooth. Recently, MD using the Tsallis statistics [21,22] has been developed and applied to chemical systems [23–25]. The Tsallis distribution, an extension of the BG distribution by one parameter q, can be realized by a certain ordinary differential equation (ODE) [26–28]. In our previous work, we proposed Tsallis dynamics (TD) [27] and declared that TD gives accurate results effectively in peptide systems and in stiff systems for which conventional method often failed in generating effectually the correct BG distributions [29,30]. When we used this equation as a sampling tool, however, we encountered a problem in determining which parameter values (including that of q) would provide the most efficient results. On the other hand, a common advantage of these methods is that they can provide BG distribution at any temperature by a reweighting technique [31], as long as they present certain defined distributions.

Now, as stated above, a common issue in developing these methods is how to determine effective values of the required parameters. A direct solution to this is to construct a protocol to find the best candidate values in each original method. These lines of investigation have been explored previously, e.g., Refs. [32,33]. Another approach is to develop a sampling method having no parameters or a method containing parameters obtained either with less effort or by a certain theoretical guide. In this paper, we consider a new sampling technique in MD that takes the latter approach. Notice that, due to the change in the parameter value, the covering region in the phase space (the covering of the potential-energy space is particularly targeted) obtained in a finite-time simulation is usually, and sometimes drastically, varied even when the change is subtle [34]. Thus, if we have to choose one value for the parameter, we are obligated to very precise setting. However, if we can realize a distribution that is a

summation of each distribution described by a distinct parameter value, we will be free from such a choice, and a broader region can be covered. Our strategy here is not to choose one distribution, but to gather the distributions together. This can succeed when the overlap of each distribution is not very small. In fact, when the distributions are associated with the parameter values of a certain fixed distribution, we should establish a suitable series of values for which the sum of these distributions makes for good sampling.

To keep a sufficient overlap of each distribution the Tsallis distributions are useful [35], since they have broad distributions. The value of the Tsallis distribution with $q>1$ exhibits slow decay with an increase in a system energy, compared with the exponential decline for the BG distribution. In general, the fundamental role of the Tsallis distribution for use in the sampling is to utilize this feature. First, this probability distribution feature enables the system governed by this distribution to escape more effectively from traps in a local region surrounded by high-energy walls. For example, the sampling behavior under use of the Tsallis distribution with $1\leqslant q\leqslant 3$ in low-dimensional potential energy systems have been discussed in detail [23,27,29,30], indicating that the distribution with $q>1$ provides faster sampling speed than that for the BG distribution (i.e., $q=1$), and thus it brings a more statistically stable distribution. However, as discussed above, the problem due to the use of only one Tsallis distribution is that the total sampling behavior often depends strongly on the choice of the values of the Tsallis distribution parameters. Nevertheless, the slow decay feature for the distribution is again helpful in order to carry out the above plan by gathering the Tsallis distributions, because the feature can be used to establish desired sufficient overlaps among mutual distribution, as demonstrated above. For these reasons, we attempt to use multiple Tsallis distribution (i) for conducting further effective escape from local traps and (ii) for smoothly realizing the strategy of gathering distributions.

We propose a deterministic scheme to realize a summation of arbitrary distributions under an ergodic assumption. To achieve this, we use density dynamics [27], which has been developed to realize any density function on the basis of the Nosé-Hoover method [36,37]. In contrast to REMD, our scheme employs a static view of the composition of distributions. Thus, in the present scheme, a jump toward a distinct phase space region dominant in each distribution occurs automatically without any change in system parameter values according to a certain periodical timing, implying that this method is free from the artifacts that depend on the choice of such a timing. Furthermore, an increase in the number of treated distributions does not indicate growth in the corresponding computational resources. Since the density of states Ω is not directly handled in this method, an assumption that Ω is smooth is not required. Of course, this method enables us to reweight the original distribution into any explicitly given distributions, because the original distribution is described definitely.

In Sec. II, we review the density dynamics and present an equation for realizing a summation of multiple arbitrarily given distributions. To illustrate our method, we performed numerical simulations for "multi-Tsallis" distributions. In Sec. III A a one-dimensional problem is treated, allowing a rigorous inspection of our method. In Sec. III B we apply our method to an alanine peptide system and discuss several realistic techniques for summing up Tsallis distributions. Our results are summarized in Sec. IV.

II. METHOD

A. Density dynamics

Let us briefly review density dynamics [27]. Consider a targeted arbitrary density function ρ (that is smooth, positive, and integrable) defined on a domain Γ in $\mathbf{R}^N$. Density dynamics defines an ODE in Γ, $\dot{\omega}=X(\omega)$, which has an invariant density ρ with respect to Lebesgue measure $d\omega$ on $\mathbf{R}^N$. On the basis of the Nosé-Hoover method [36,37], we employed the following ODE with $N\equiv 2n+1$:

$$\begin{aligned}
\dot{x}_i &= D_{p_i}\Theta(\omega), \quad i=1,\ldots,n,\\
\dot{p}_i &= -D_{x_i}\Theta(\omega) - D_{\zeta}\Theta(\omega)p_i, \quad i=1,\ldots,n,\\
\dot{\zeta} &= \sum_{j=1}^{n} D_{p_j}\Theta(\omega)p_j - nT,
\end{aligned} \tag{1}$$

where $\Theta\equiv -T\ln\rho:\Gamma\to\mathbf{R}$; $D_{x_i}\Theta(\omega)$, $D_{p_i}\Theta(\omega)$, and $D_{\zeta}\Theta(\omega)$ denote the partial derivatives of Θ at point $\omega\equiv(x,p,\zeta)$ with respect to x_i, p_i, $(i=1,\ldots,n)$ and ζ, respectively. Here, as pointed out in Ref. [27], we have multiplied X by a factor T having an energy dimension to set each variable's dimension as a physically natural one: x_i is a coordinate and p_i a momentum.

Under the assumption that X is complete, it is shown that, by Birkhoff's individual ergodic theorem, a time average of any function f (assume, also below, e.g., a Borel measurable function on Γ with $\int_\Gamma |f\rho|d\omega<+\infty$) has a long-time limit value for $(\rho d\omega)$ almost every initial point. Further, if the flow is ergodic with respect to measure $\rho d\omega$,

$$\lim_{\tau\to\infty}\frac{1}{\tau}\int_0^\tau f(\omega(t))dt = \int_\Gamma f(\omega)\rho(\omega)d\omega \Big/ \int_\Gamma \rho(\omega)d\omega \tag{2}$$

holds almost everywhere. Substitution of $f\equiv\chi_A$, the characteristic function for an area $A\subset\Gamma$, gives the interpretation that the probability density for the realization of point ω is proportional to the given value $\rho(\omega)$.

B. Realization of summation of arbitrary densities

We apply Eq. (1) to realize a summation of M arbitrary densities. Let $\rho^a:\Gamma\to\mathbf{R}$, $a=1,\ldots,M$, be the density functions that will be summed up. Since a physical system is usually represented by potential energy $U(x)$ and kinetic energy $K(p)$ [let U be a smooth function on a domain $V\subset\mathbf{R}^n$ and $K(p)\equiv\frac{1}{2}\|p\|^2$], we here take the form

$$\rho^a(x,p,\zeta)\equiv\rho_P^a(U(x),K(p))\rho_z(\zeta), \tag{3}$$

where ρ_P^a and ρ_z are smooth, positive functions on certain sets in $\mathbf{R}^2$ and $\mathbf{R}$, respectively. A summation of the densities

$$\rho(\omega) \equiv \sum_{a=1}^{M} \rho^a(x,p,\zeta), \tag{4}$$

where we set $\omega=(x,p,\zeta)\in\Gamma\equiv V\times\mathbf{R}^n\times\mathbf{R}$, can be realized in the sense stated in Sec. II A when we substitute Eq. (4) into Eq. (1), this substitution yielding

$$\dot{x}_i = \tau_2(x,p)p_i, \quad i=1,\ldots,n, \tag{5}$$

$$\dot{p}_i = -\tau_1(x,p)D_iU(x) - \tau_3(\zeta)p_i, \quad i=1,\ldots,n, \tag{6}$$

$$\dot{\zeta} = \tau_2(x,p)\|p\|^2 - nT, \tag{7}$$

where

$$\tau_\alpha(x,p) \equiv -TD_\alpha\left[\ln\sum_{a=1}^{M}\rho_P^a\right](U(x),K(p)) = -T\frac{\sum_{a=1}^{M} D_\alpha\rho_P^a(U(x),K(p))}{\sum_{a=1}^{M}\rho_P^a(U(x),K(p))}, \quad \alpha=1,2, \tag{8}$$

$$\tau_3(\zeta) \equiv -TD\ln\rho_z(\zeta). \tag{9}$$

Here, $D_\alpha f(u,k)$ is the partial derivative of function f at point (u,k) with respect to the α (1 or 2)th component, viz., u or k, and $D\ln\rho_z(\zeta)$ is the derivative of $\ln\rho_z$ at ζ. First, we note that this equation requires nearly the same computational cost as the conventional MD equations do. In a typical MD simulation, most of the time is consumed in calculating $U(x)$ and $D_iU(x)$. Once we get the $U(x)$ value, the summation appearing in Eq. (8), even for a large M, takes much less computational overhead than that of $U(x)$, as long as the cost of calculating the values for the two-variable functions ρ_P^a and $D_\alpha\rho_P^a$ is low (as it usually is). Moreover, the ODE does not need the derivative of the density of states, so that an assumption of the smoothness is not requisite in our method.

We should often consider cases where each ρ^a is normalized. That is, we have to treat

$$\rho \equiv \sum_{a=1}^{M}\overline{\rho^a} \tag{10}$$

with $\overline{\rho^a}\equiv\rho^a/Z^a$, where $Z^a\equiv\int_\Gamma\rho^a(\omega)d\omega$ $(a=1,\ldots,M)$. However, calculating an absolute value of the partition function Z^a is, in general, very hard. To make it easier, we use

$$\tilde{\rho} \equiv \sum_{a=1}^{M}\rho^a/Y^a = Z^c\rho, \tag{11}$$

in place of Eq. (10), where $Y^a\equiv Z^a/Z^c$, c being an arbitrary fixed value in $\mathcal{M}\equiv\{1,\ldots,M\}$ [we can weaken the assumption that $Z^a<\infty$ for all $a\in\mathcal{M}$; then component a with $Z^a=\infty$ just makes no contribution to the sum or the ODE, provided that $Z^c<\infty$; see Eq. (12) below]. The value of Y^a can be calculated or estimated as described below. The resulting change in Eqs. (5)–(9) is only in Eq. (8), given by

$$\tau_\alpha(x,p) = -T\frac{\sum_{a=1}^{M} D_\alpha\rho_P^a(U(x),K(p))/Y^a}{\sum_{a=1}^{M}\rho_P^a(U(x),K(p))/Y^a}, \quad \alpha=1,2, \tag{12}$$

and from the assumptions of the ergodicity for $\tilde{\rho}$ [38] and the completeness we have

$$\lim_{\tau\to\infty}\frac{1}{\tau}\int_0^\tau f(\omega(t))dt \tag{13}$$

$$= \int_\Gamma f\tilde{\rho}d\omega \Big/ \int_\Gamma\tilde{\rho}d\omega \tag{14}$$

$$= \int_\Gamma f\rho d\omega \Big/ \int_\Gamma\rho d\omega \equiv \langle f\rangle, \tag{15}$$

as in Eq. (2). So we get the required results denoted by objective density ρ of Eq. (10). It should be noted that the expectation value $\langle f\rangle$ becomes an average of each of the corresponding expectations $\langle f\rangle^a\equiv\int_\Gamma f\rho^a d\omega/Z^a$,

$$\langle f\rangle = \frac{1}{M}\sum_{a=1}^{M}\langle f\rangle^a, \tag{16}$$

as is clear from $\int_\Gamma f\rho d\omega=\int_\Gamma d\omega\Sigma_{a=1}^M f\rho^a/Z^a=\Sigma_{a=1}^M\langle f\rangle^a$ and $Z\equiv\int_\Gamma\rho d\omega=\Sigma_{a=1}^M\langle 1\rangle^a=M$. Likewise, by putting $f\equiv\chi_A$, the probability for realizing area $A\subset\Gamma$, $P(A)\equiv\int_A\rho d\omega/\int_\Gamma\rho d\omega$, is an average of each of the corresponding probabilities $P^a(A)\equiv\int_A\rho^a d\omega/Z^a$. Namely, we have derived the averaged (or summed, up to the normalization) measure from each probability measure (for Borel sets in Γ) P^a.

A practical way to calculate Y^a is to proceed as follows. (i) Rearrange given $\overline{\rho^1}, \overline{\rho^2}, \ldots, \overline{\rho^M}$, using a permutation $\sigma:\mathcal{M}=\{1,\ldots,M\}\to\mathcal{M}$, such that the overlap between $\overline{\rho^{\sigma^{-1}(a')}}$ and $\overline{\rho^{\sigma^{-1}(a'+1)}}$ is sufficient for all $a'=1,\ldots,M-1$. (ii) Estimate the rate of partition functions for each neighboring pair, resulting in, for example, $c=1$ with

$$Y^{\sigma^{-1}(a')} = \begin{cases} \prod_{j=\sigma(1)+1}^{a'} Z^{\sigma^{-1}(j)}/Z^{\sigma^{-1}(j-1)} & \cdots a' > \sigma(1), \\ 1 & \cdots a' = \sigma(1), \\ \prod_{j=a'+1}^{\sigma(1)} Z^{\sigma^{-1}(j-1)}/Z^{\sigma^{-1}(j)} & \cdots a' < \sigma(1) \end{cases}$$

for $a'\in\mathcal{M}$. These partition function rates can be estimated by the free-energy perturbation (FEP) method [39] or the thermodynamic integration method [40] or by advanced approaches [41] based on them.

However, it remains difficult to achieve accurate values for partition function rates in actual complicated systems. Here, it should be emphasized that our final goal is not to obtain accurate values of Y^as, but to generate an appropriate combination of each distribution such that an effective sampling of states is achieved. In other words, any $\{Y^a\}_{a\in\mathcal{M}}$

defines a certain density (thus permitting reweighting) in principle and so is sufficient whenever we have good sampling as a result of this method (viz., to obtain accurate $\{Y^a\}$ is not a necessary condition but a sufficient condition to achieve good sampling, as long as we assume that $\rho = \Sigma_{a=1}^{M} \rho^a / Z^a$ causes such a sampling). For this reason, in Sec. III we study the dependence of the results on the value of Y^a in numerical simulations.

Potential function distribution is an often targeted matter. It is thus useful to know how the potential distribution for the current sum of the given densities $\rho^1, \ldots, \rho^M$ is represented by that for each ρ^a. Let $\{T_t : \Gamma \to \Gamma \,|\, t \in \mathbf{R}\}$ be the flow generated by Eqs. (5)–(7), (9), and (12). Under the ergodic assumption with suitable additional mathematical conditions, we can show that the probability distribution density of potential function, P_U, at a point u is represented by

$$\begin{aligned} P_U(u) &\equiv \lim_{|I|\to 0} \frac{\lim_{\tau\to\infty} \frac{1}{\tau}\int_0^\tau \chi_{U^{-1}(I)} \circ \pi_1 \circ T_t(\omega) dt}{|I|} \\ &= \lim_{|I|\to 0} \frac{1}{|I|} \int_\Gamma \chi_{U^{-1}(I)}(x) \rho(\omega) d\omega / Z \\ &= \sum_{a=1}^{M} \rho^{a,1}(u) \Omega_U(u) / M, \end{aligned} \tag{17}$$

almost surely, where $I \subset \mathbf{R}$ is a bin associated to u [42], π_1 is a projection: $\omega \mapsto x$, $\chi_{U^{-1}(I)}(x)$ takes 1 [0] if $U(x) \in I$ [otherwise], $\rho^{a,1}(U(x)) \equiv \int_{\mathbf{R}^{n+1}} \rho^a(x,p,\zeta) dp d\zeta$, and Ω_U is the density of states for U. For the potential function distributions for ρ^a, we now assume similar conditions, so each flow $\{T_t^a \,|\, t \in \mathbf{R}\}$ [which can be constructed by putting $\mathcal{M} \equiv \{a\}$] having an invariant density ρ^a is ergodic with respect to $\rho^a d\omega$ for $a \in \mathcal{M}$. Then, we also have

$$P_U^a(u) \equiv \lim_{|I|\to 0} \frac{\lim_{\tau\to\infty} \frac{1}{\tau}\int_0^\tau \chi_{U^{-1}(I)} \circ \pi_1 \circ T_t^a(\omega) dt}{|I|} = \rho^{a,1}(u) \Omega_U(u). \tag{18}$$

Hence we get

$$P_U(u) = \frac{1}{M} \sum_{a=1}^{M} P_U^a(u), \tag{19}$$

showing that the probability density for U taking a value of u with respect to $\{T_t\}$ is given by the average of the corresponding densities with respect to $\{T_t^1\}, \ldots, \{T_t^M\}$.

C. Dynamics for multi-Tsallis distribution

As is often observed through a long tail in energy distribution (especially on the high-energy side) [34], effective support of the Tsallis distribution with $q > 1$ is broad compared with that of the BG distribution. This characteristic is convenient for making overlaps among the distributions so as to evaluate Y^a safely, as discussed in Sec. II B. Therefore we consider a dynamics that realizes a summation of Tsallis distributions, which we have called multi-Tsallis distribution.

One manner for conducting this is to use the form of

$$\rho_E^a(e) \equiv [1 + \alpha_a(e + \varepsilon_a)]^{b_a}, \tag{20}$$

by recasting it as $\rho_P^a(U(x),K(p)) \equiv \rho_E^a(E(x,p))$ with $E(x,p) \equiv U(x) + K(p)$ in Eq. (3), which results in an ODE defined by Eqs. (5)–(7) and (9), and

$$\tau_1(x,p) = \tau_2(x,p) = -T \frac{\sum_{a=1}^{M} D\rho_E^a(E(x,p))/Y^a}{\sum_{a=1}^{M} \rho_E^a(E(x,p))/Y^a}. \tag{21}$$

That is, we can realize the multi-Tsallis distribution denoted by the density (up to the normalization constant)

$$\sum_{a=1}^{M} \rho_P^a(U(x),K(p))/Z'^a = \sum_{a=1}^{M} [1 + \alpha_a(E(x,p) + \varepsilon_a)]^{b_a}/Z'^a, \tag{22}$$

where $Z'^a \equiv \int_{\Gamma'} \rho_P^a(U(x),K(p)) dx dp$, noting that

$$\begin{aligned} &\int_\Gamma O(x,p) \rho(\omega) d\omega / Z \\ &= \int_{\Gamma'} O(x,p) \sum_{a=1}^{M} \rho_P^a(U(x),K(p))/Z'^a dx dp \Big/ \\ &\quad \int_{\Gamma'} \sum_{a=1}^{M} \rho_P^a(U(x),K(p))/Z'^a dx dp \end{aligned}$$

holds for $O : \Gamma' \equiv V \times \mathbf{R}^n \to \mathbf{R}$ with $\int_\Gamma |O\rho| d\omega < +\infty$. Here, our main concern is for $\alpha_a \equiv (q_a - 1)/T_a$ and $b_a \equiv 1/(1-q_a)$ [while this form was used in the following numerical simulations, $b_a \equiv q_a/(1-q_a)$ can also be considered [43]] ($a \in \mathcal{M}$); q_a is the Tsallis index (we set $q_a > 1$), $T_a > 0$ is the temperature parameter, and ε_a is a shift parameter so that we should ensure $1 + \alpha_a(e + \varepsilon_a) > 0$ for accessible e values in order to define Eq. (20) well [22,44,45]. In Sec. III, by the formulation described so far, we examine a realization of the distribution of Eq. (22). Note that a choice of $M \equiv 1$ means a single Tsallis distribution and also reduces the ODE defined by Eqs. (5)–(7), (9), (20), and (21) [with $\alpha_1 \equiv (q-1)/T$, $\varepsilon_1 \equiv 0$, and $b_1 \equiv q/(1-q)$] to the TD equation [27,29]. The present equation is hence an extension of the TD.

Another density with which we employ the Tsallis form may be

$$\rho_P^a(u,k) \equiv [1 + \alpha_a(u + \varepsilon_a)]^{b_a} \exp(-\beta_a k). \tag{23}$$

This splitting form for U and K denotes that the potential energy obeys the Tsallis distribution while the kinetic energy obeys the BG distribution at temperature $1/\beta_a$. It should be noted that the temperature $1/\beta_a$ can take a different value for each a, suggesting a scheme encouraging an efficient sampling: for a such that the potential energy covering region (governed by $[1 + \alpha_a(u + \varepsilon_a)]^{b_a}$) is mainly located in a lower

energy side, we can use a high $1/\beta_a$ to induce large fluctuations for escaping traps.

III. NUMERICAL SIMULATION

We investigate the realization of the multi-distribution defined by Eq. (22) via Eqs. (5)–(7), (9), (20), and (21) through numerical simulations with the use of the fourth-order Runge-Kutta integration method. Section III A treats a low-dimensional system to compare the results obtained from our scheme with the exact values. Section III B treats a peptide molecule system and demonstrates several technical issues involved in the realistic effective sampling.

A. One-dimensional double-well potential model

A model system of a one-dimensional double-well (1DW) potential

$$U(x) = D(x^2 - 1)^2 \tag{24}$$

was applied. Despite the simplicity of the form, this potential thrusts the conventional MD simulation into local traps and often leads to a failure to correctly sample the states of the system [46,47], and yet its density of states is not smooth.

All variables were treated as dimensionless, and the following simulation conditions were used. The barrier height of the potential was $D=5$; $\tau_3(\zeta)=500\zeta$ was used for the density for ζ along with the scaling factor of $T=10$; and the total time steps and the unit step Δt were 10^8 and 5×10^{-4}, respectively. Initial values for the ODE were $x(0)=0$, $p(0)=1$, and $\zeta(0)=0$.

We here exhibit the results of two kinds of summation of Tsallis distributions for this system. First, we show the sum using two different values for the Tsallis index and the same values for the temperature parameter [Eq. (22) with $M=2$]: $q_1=1.5$, $q_2=2$; $T_1=T_2=1$. Note that we chose the values in that Z^1, $Z^2<\infty$; and we set $\varepsilon_1=\varepsilon_2=0$ because $U\geqslant 0$ is explicitly ensured. The partition function rate was obtained in a straightforward manner from

$$\begin{aligned} Z^a &= \int_{\mathbf{R}^3} [1 + \alpha_a(K(p) + U(x) + \varepsilon_a)]^{b_a} \rho_z(\zeta) dx dp d\zeta \\ &= \left[\gamma \Gamma(-b_a - 1/2) \Big/ \sqrt{\alpha_a}\Gamma(-b_a)\right] \\ &\quad \times \int_{\mathbf{R}} [1 + \alpha_a(U(x) + \varepsilon_a)]^{b_a+1/2} dx \end{aligned}$$

(valid for $n=1$, $V=\mathbf{R}$, $-b_a>1/2$, and $U>-1/\alpha_a-\varepsilon_a$) with its evaluation, where γ is a constant irrelevant to a and $\Gamma(\cdot)$ is the gamma function. Figure 1 shows the distribution density of coordinate x, f_1, and that of momentum p, f_2. To understand the situation well, we draw an exact density for the single Tsallis distribution with $q=1.5$, $T=1$ and that with $q=2$, $T=1$; the latter is flatter than the former, driven by the larger q effect [23]. For the multi-Tsallis distribution [Eq. (22)], its exact $f_1[f_2]$ is shown to be equal to the average of above each exact $f_1[f_2]$, as indicated in the figure. We show the simulation results obtained by the current method for this multidistribution and its very good agreement with the exact values.

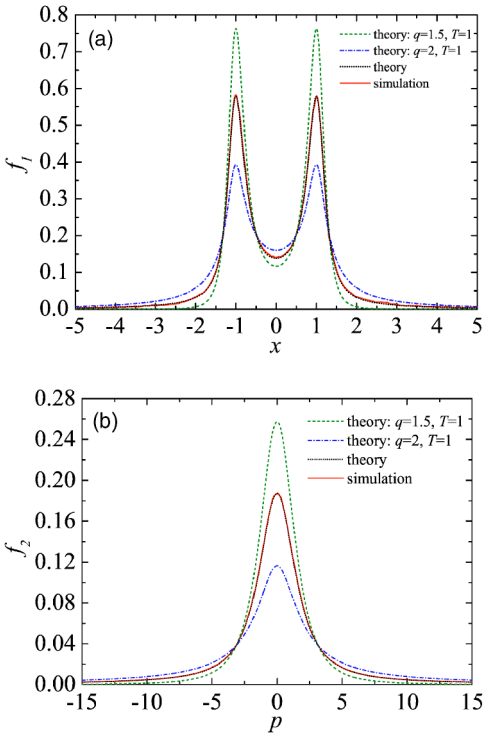

FIG. 1. (Color online) Distribution density of coordinate x (a) and momentum p (b) for 1DW. The theoretical values for single Tsallis distribution with $q=1.5$, $T=1$ and that with $q=2$, $T=1$ are indicated by dashed and dash-dotted lines, respectively. Theoretical values and simulated results (the bin sizes of the histograms were 0.02) for the multi-Tsallis distribution defined by the sum of these two distributions are shown by dotted and solid lines, respectively.

Second, Fig. 2 presents the sum obtained from the use of different values for the temperature parameter and the same values for the Tsallis index: $q_1=q_2=1.5$; $T_1=1$, $T_2=10$. Again, the simulation results for this multidistribution agreed quite well with the theoretical values. We also varied the coefficient for the "friction" relevant term in Eq. (6), which has often been discussed in the Nosé-Hoover equation type [48,49], as $\tau_3(\zeta)/\zeta=20$, 50, 100, 200, 500, and 1000, and obtained similar results. Consequently, these results confirm that the current method provides accurate multidistributions that were constituted in different manners using distinct parameter-set values.

To confirm Eq. (17) directly, we examined the potential energy distribution density $P_U(u)$, as depicted in Fig. 3. Here, the theoretical value in this case is represented by $(1/M)\Sigma_{a=1}^{M}\rho^{a,1}(u)\Omega_U(u)$ for $u\in(0,D)\cup(D,\infty)$ with

$$\rho^{a,1}(u) = [1 + (u + \varepsilon_a)(q_a - 1)/T_a]^{1/(1-q_a)+1/2}/\tilde{Z}^a,$$

where $\tilde{Z}^a \equiv \int_{\mathbf{R}}[1+(U(x)+\varepsilon_a)(q_a-1)/T_a]^{1/(1-q_a)+1/2}dx = \int_0^\infty[1+(u+\varepsilon_a)(q_a-1)/T_a]^{1/(1-q_a)+1/2}\Omega_U(u)du$ is a normalization constant, and

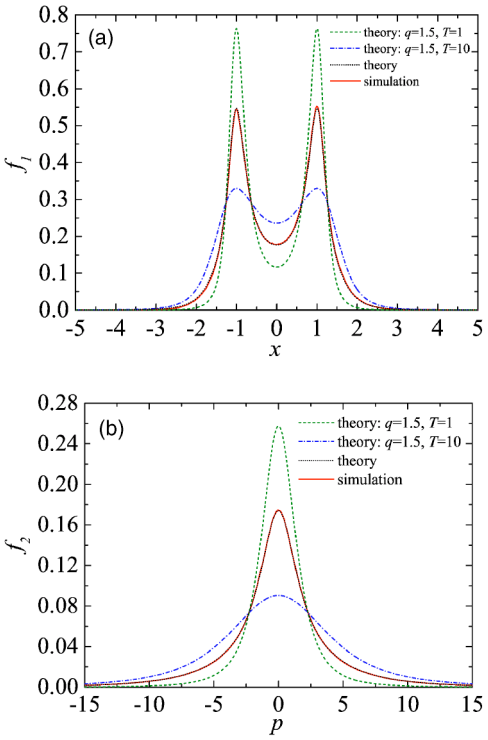

FIG. 2. (Color online) Distribution density of coordinate x (a) and momentum p (b) for 1DW. The theoretical value for single Tsallis distribution with $q=1.5$, $T=1$ and that with $q=1.5$, $T=10$ are indicated by dashed and dash-dotted lines, respectively. Theoretical values and simulated results (the bin sizes of the histograms were 0.02) for the multi-Tsallis distribution defined by the sum of these two distributions are shown by dotted and solid lines, respectively.

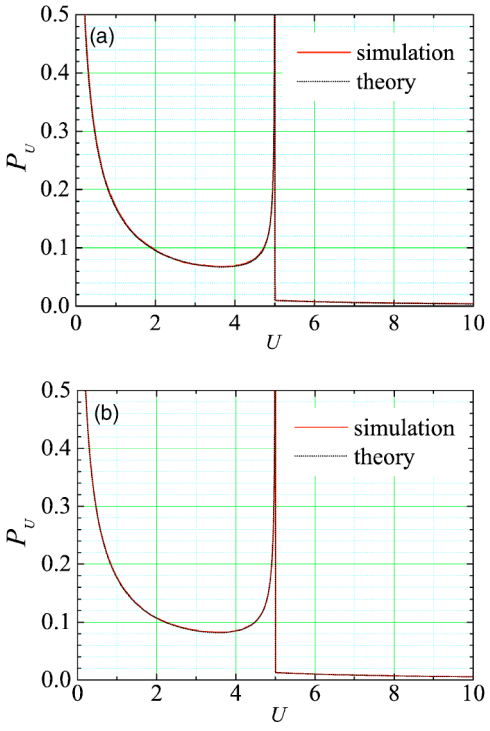

FIG. 3. (Color online) Distribution density of potential energy for 1DW for the multi-Tsallis distribution defined by (a) $q_1=1.5$, $q_2=2$; $T_1=T_2=1$ and (b) $q_1=q_2=1.5$; $T_1=1$, $T_2=10$. Solid and dotted lines indicate the simulated value (the bin sizes of the histograms were 0.01) and the theoretical value, respectively.

$$\Omega_U(u) \equiv \frac{d}{du}\int_{\{y|U(y)\leqslant u\}} dx = \begin{cases} \dfrac{1}{2\sqrt{D}}[h_+(u)+h_-(u)], & 0<u<D, \\ \dfrac{1}{2\sqrt{D}}h_-(u), & u>D, \end{cases}$$

where $h_\pm(u) \equiv [u(\mp\sqrt{u/D}+1)]^{-1/2}$. The exceptional points for Ω_U are $u=0$ and $u=D$, which are critical values of U; any definitions of $\Omega_U(0)$ and $\Omega_U(D)$ must admit discontinuities of Ω_U at these points. The agreement in P_U between the theoretical values and the simulation results [the left-hand side of Eq. (17) was estimated] clearly shows that indeed the current method does not require a smooth density of states.

B. Alanine tripeptide system

For protein simulation based on all-atom model, we performed a benchmark test using a simple alanine peptide system, as applied in fundamental investigations [7,33,35,50]. We used Ac-Ala-Ala-NMe, which is composed of 32 atoms, where Ac and NMe are acetyl and N-methyl groups, respectively. In general, even if a peptide system is small, it can be complicated, and several interesting phenomena have been observed: for instance, the energy landscape often possess many local minima due to the complicated feature of the interactions, and from an experiment interesting kinetic conformational isomerization has been indicated [51]. Alanine tripeptide system is one of the most simplest peptides that can form the reverse turn, which is an important secondary structural element in folded proteins [52]. Existing free-energy barrier in the system between the reverse turn (folded) conformation and the extended (unfolded) conformation is more than about 3 kcal/mol [20,30,52], and thus regular MD simulation at low temperature often leads to insufficient sampling results within a typical simulation period.

The C96 AMBER force field for all atom version [53,54] was used, which consists of bond and angle stretch, dihedral rotations, and both the van der Waals and electrostatic nonbonded interactions. We set the dielectric constant to 1 and used no cutoff for the nonbonded interactions. An extended conformation was taken as a molecule's initial structure. The ODE parameters were set to $\rho_z(\zeta) \equiv \exp(-c\zeta^2)$ with $c=10^4$ $(\mathrm{g/mol})^{-2}$ $\mathrm{\AA}^{-4}$ fs^2 and $T=200$ K. The simulations of 5×10^7 time steps using $\Delta t=0.1$ fs were performed by the program PRESTO [55,56] with a modification for the current method.

Although an ad hoc manner to set the Tsallis parameter values led to success in the 1DW case, a system with a large phase space requires an intensively suitable manner with which we establish a setting for effective sampling within a restricted finite time. We approach such a manner by considering the generation of an adequate parameter sequence to

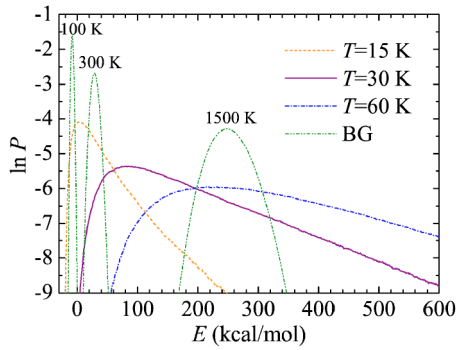

FIG. 4. (Color online) Distribution density of the total energy of the alanine tripeptide system. The results shown are for single Tsallis distributions at the indicated values of the T parameter; also shown for comparison are for the BG distributions at 100, 300, and 1500 K.

build an effective multidistribution (Sec. III B 1), before describing the simulation results (Sec. III B 2).

1. Protocol

The following scheme was used to generate the parameter sequence. The parameters ε_a and q_a were fixed for all a, and so each distribution was summed up with the use of a different value of parameter T_a. We used $\varepsilon \equiv \varepsilon_1 = \cdots = \varepsilon_M = -\tilde{U}_{\rm inf}$, a minus value of a candidate of the infimum of U. This setting is an easy way to ensure $1+(q_a-1)(U(x)+K(p)+\varepsilon_a)/k_B T_a > 0$ for all a. A not-so-serious choice of $\tilde{U}_{\rm inf}$ for this assurance may be required in our case, since the term "$+K(p)$" gives a certain amount of the margin. We estimated that $\tilde{U}_{\rm inf} = -25$ kcal/mol, which was the minimum of the potential energy value obtained in the presimulation on a conventional Boltzmann-Gibbs MD simulation at 50 K. For q, we employed the Hansmann-Okamoto strategy [57], which was previously obtained using a harmonic approximation in energy expectation for a single Tsallis distribution. That is, we set $q \equiv q_1 = \cdots = q_M = 1+1/n$, where n is the number of degrees of freedom for the system. In fact, we have also found that this setting easily allows a significantly wide region sampling, especially in comparison with BG distributions. Thus, this value is expedient for our purpose. To set the values of T_a, we previously calculated the single (not multiple) distribution defined by (q, ε, T_a) for several T_a, using the TD method [27]. The results of the total energy distribution are shown in Fig. 4. We can observe that the distribution with $T_a = 15$ K and that with $T_a = 60$ K have a certain amount of overlap with each other, and the sum of only these two distributions is expected to have a wide covering region. Accordingly, we decided that $M=2$ with $(q_1, \varepsilon_1, T_1) = (q, \varepsilon, 15)$ and $(q_2, \varepsilon_2, T_2) = (q, \varepsilon, 60)$.

To perform smoothly this protocol for setting the value of T_a, it is convenient to use a certain reference value for T_a in advance. If we get such a value, we can use the TD to perturb T_a around this value in order to decide the manner on a summation. This proposal is based on the observation that the "weight" of the Tsallis energy distribution density usually shifts toward the high-energy region, as increasing T in $\rho_E(e) \equiv [1+(q-1)(e+\varepsilon)/k_B T)]^b$. In view of the energy expectation, this observation can be supported when, for example, we assume a simple approximate form for the density of states as $\Omega(e) = r(e-E_{\rm inf})^\nu$ for a certain r, $\nu \in \mathbf{R}$ [57]. If we suppose $-b > \nu+2 > 1$, then we obtain

$$\langle E \rangle \equiv \int_{E_{\rm inf}}^{\infty} de \Omega(e) \rho_E(e) e \Big/ \int_{E_{\rm inf}}^{\infty} de \Omega(e) \rho_E(e) = k_B T [1 + (q-1)(E_{\rm inf} + \varepsilon)/k_B T] \mu(q) + E_{\rm inf}, \quad (25)$$

where $\mu(q) \equiv [1/(q-1)][(\nu+1)/(-b-\nu-2)] > 0$, showing that the energy expectation in the Tsallis distribution increases with respect to T within a range in which the approximation makes sense.

Here we introduce one practical method for giving a rough theoretical estimate of the reference value for temperature T_a. Regarding the BG energy distribution density $P_{\rm BG} > 0$, assume that $\ln P_{\rm BG}$ is concave and that $P_{\rm BG}(E_1) = P_{\rm BG}(E_2)$ holds for certain energy values of $E_1 < E_2$. It follows from these assumptions that $E_1 \leqslant E_{\rm BG}^{\max} \leqslant E_2$, where $E_{\rm BG}^{\max}$ is the maximum point of $\ln P_{\rm BG}$ [58]. Also suppose the concavity condition for the (single) Tsallis energy distribution density $P > 0$ associated with (q, ε, T). Then, the validity of $P(E_1) = P(E_2)$ results in $E_1 \leqslant E^{\max} \leqslant E_2$, $E^{\max}$ being the maximum point of $\ln P$, meaning that the effective support of $\ln P$ can cover the major region covered by $\ln P_{\rm BG}$ (e.g., a usual target is the region covered by $P_{\rm BG}$ at room temperature). Thus, the parameter value that provides $P(E_1) = P(E_2)$ can be used as a reference value. Now we can directly show that the relation $P(E_1) = P(E_2)$, employing $P = \rho_E \Omega / Z'$ and $P_{\rm BG} = \rho_E^{\rm BG} \Omega / Z'_{\rm BG}$ [here, $\rho_E^{\rm BG}(e) \equiv \exp(-\beta e)$, Z' and $Z'_{\rm BG}$ are normalization constants, and Ω is the density of states (of any form)], is equivalent to the following:

$$T = T_{\rm ref} \equiv \frac{1-q}{k_B} \frac{(E_2+\varepsilon)\exp\left(\frac{\beta}{b}E_2\right) - (E_1+\varepsilon)\exp\left(\frac{\beta}{b}E_1\right)}{\exp\left(\frac{\beta}{b}E_2\right) - \exp\left(\frac{\beta}{b}E_1\right)}. \quad (26)$$

Using the values for q and ε defined at the beginning of Sec. III B 1 and putting $b \equiv 1/(1-q)$, Eq. (26) can present the sought-for reference value. In fact, we have obtained $T_{\rm ref} = 19.9$ K through the following choice of E_1, E_2, and β: we set $1/k_B\beta = 300$ K; from the simulated results of the BG total energy distribution at β we chose $E_2 \equiv \langle E \rangle_{\rm BG} + \sigma_{\rm BG}$ (the average BG energy plus the standard deviation) and determined E_1 so that $P_{\rm BG}(E_1) = P_{\rm BG}(E_2)$ holds. Figure 5 shows the simulation results of $P_{\rm BG}$ at 300 K and that of P at 19.9 K. The validity of $P(E_1) = P(E_2)$ was quite good, and the effective support of $\ln P$ sufficiently covers that of $\ln P_{\rm BG}$, indicating the cogency of the present method.

Now, unlike the case of the 1DW, the partition function rate cannot be evaluated simply; even when we use for instance the FEP, it does not completely give the correct answer within an actual computation period against a complicated system [59]. From the standpoint stated in Sec. II B, however, we do not necessarily need to pursue the accuracy.

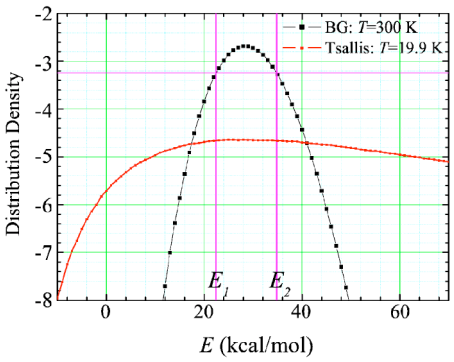

FIG. 5. Total energy distribution density of the alanine system for the BG distribution at 300 K, P_{BG}, and that for the Tsallis distribution at $T=19.9$ K; their logarithm values are shown. E_1 and E_2 were chosen so that $P_{\mathrm{BG}}(E_1)=P_{\mathrm{BG}}(E_2)$ holds.

Thus, instead of employing the FEP or some elaborated method, we here used a very simple relation for the estimate,

$$(P^a(E)/P^b(E))(\rho_E^b(E)/\rho_E^a(E)) = Z^b/Z^a, \tag{27}$$

where P^a is the energy distribution density produced from $\rho_E^a > 0[\rho^a(x,p,\zeta) \equiv \rho_E^a(E(x,p))\rho_z(\zeta)]$, and P^b is similar along with $P^b(E) \neq 0$. In a typical case, a point E_0 such that $P^a(E_0)=P^b(E_0)$ may bring a reliable statistical result, since both P^a and P^b attain relatively high values at the intersection point E_0 (take an appropriate criterion when E_0 is not unique; e.g., we chose one having a larger value of P^a). For these reasons, we evaluated the rate using Eq. (27) at $E=E_0$ in all the following results.

2. Simulation results

Figure 6 shows the simulation results of the potential energy distribution density for $\overline{\rho^a}$ obtained by the TD method and the distribution for their sum obtained by the current method. [We set as $M=2$ and $c=1$; $\overline{\rho^1}$ was the Tsallis density with (q,ε,T_1); $\overline{\rho^2}$ was that with (q,ε,T_2).] In this case, in contrast to the 1DW, it is difficult to obtain the exact values of the energy distribution, even for the single parameter distribution, and so it is difficult to obtain an average of the exact distributions (viz., exact answer for the current method). However, as shown in Ref. [30], the TD simulation for the single distribution must have given results with good accuracy, if the energy value was in the sufficiently attainable range; otherwise, the results is suppressed compared with the other when we take their sum (note that the current method can reach the region where either distribution is attainable). Hence, their average gives a good estimate of the theoretical value. Figure 6 shows that this average and the results by the current method were finely approximated. For these reasons, we can conclude that Eq. (19) was valid in this case and that our scheme worked well. Note that, in general, as system become large, required sampling space region grows. Thus, the corresponding sufficient simulation time is needed to obtain reasonable results. Aside from this issue lying commonly among sampling methods, in principle, the current method would have no peculiar problem against an increase in the system size. Even though we employ many distributions for covering wide region in order to tackle the issue for large systems, the computational cost to treat the ODE does not so increase (as stated in Sec. II B), compared with the cost in the case with a few distributions such as that in the present simulation.

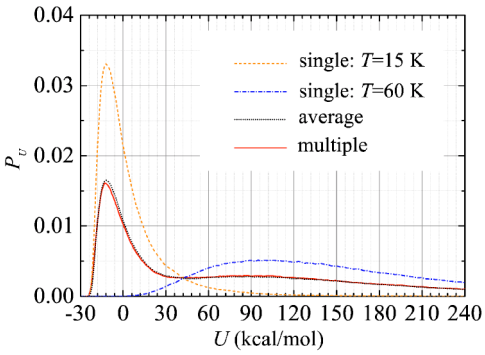

FIG. 6. (Color online) Potential energy distribution density of the alanine system. Dashed and dash-dotted lines are simulated results for the single-Tsallis distribution with $(q_1,\varepsilon_1,T_1)=(1.010416\dot{}, 25\ \mathrm{kcal/mol}, 15\ \mathrm{K})$ and that with $(q_2,\varepsilon_2,T_2)=(1.010416\dot{}, 25\ \mathrm{kcal/mol}, 60\ \mathrm{K})$, respectively. The average of these two single distributions is shown by the dotted line. The corresponding simulated results for the multi-Tsallis distribution by the current method is given by a solid line.

We sought to understand how the difference, between the current multidistribution and the conventional single distribution, was responsible for the physical results. In Fig. 7, we show the BG (both potential and kinetic) energy distributions at several temperatures, calculated by the current method as well as by the TD method for (q,ε,T_a) distribution, using the reweighting technique. Aside from the low-temperature region, single distribution with $T=15$ led to a not so statistically satisfactory answer for high temperatures; on the other hand, that with $T=60$ gave reasonable results for high temperatures but caused erroneously shrinking results in the low-temperature region. However, with the multidistribution, the low-temperature results were consistent with those obtained by the low-temperature-oriented single distribution with $T=15$, and the high-temperature results were consistent with those by the high-temperature-oriented single $T=60$ distribution. Furthermore, as for kinetic energy distributions, the current method showed very good agreement with the theoretical values [30] across the whole temperature range. These results indicate the superiority of the current method in that this method yielded statistically reasonable results for physical quantities over a wide range of temperatures, whose range was intractable with the single distribution during the same simulation period.

To compare quantitatively the efficiency of the current scheme and that of the conventional ones with the above single distributions, we measured the number of tunneling events in the potential energy trajectory, n_T. This is defined as the number of events that go from a certain energy value U_H to another value U_L and back [60], and it can be understood that the efficiency raises with progression of n_T. First, to judge efficiencies using a common attainable energy region among these schemes, we set $U_L=10$ and

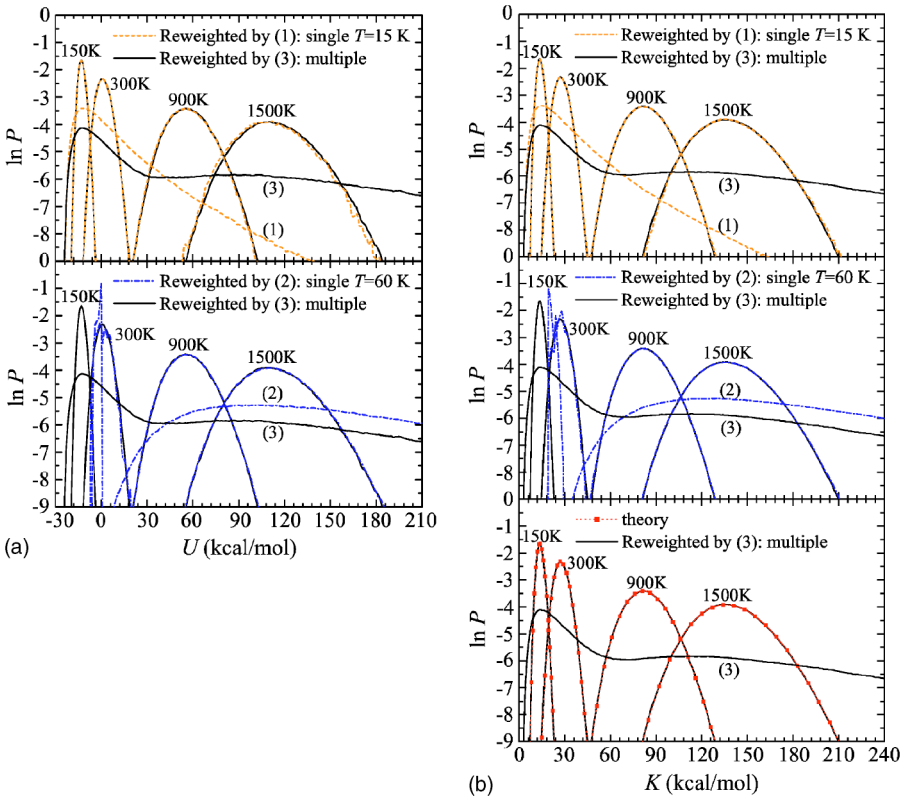

FIG. 7. (Color online) BG energy distribution densities at $T=150$, 300, 900, and 1500 K of the alanine system for potential energy (a) and kinetic energy (b). Reweighted results obtained from the simulation realizing (1) the single Tsallis distribution with (q_1,ε_1,T_1), (2) that with (q_2,ε_2,T_2), and (3) the current multi-Tsallis distribution. In (a), upper panel shows the results for (1) and (3); lower for (2) and (3). In (b), upper for (1) and (3); middle for (2) and (3); lower the results for the theoretical values and (3).

$U_H=130$ kcal/mol. They were set from the reason that the U_L value was assessed at a representative lower energy value for the high-temperature-oriented single $T=60$ Tsallis distribution from the observation that $U\simeq 8$ kcal/mol for which $\ln P(U)=-9$ holds, and likewise that the U_H a representative upper value for the low-temperature-oriented single $T=15$ distribution from $\ln P(138\ \text{kcal/mol})\simeq -9$; see Fig. 7(a). These U_L and U_H values were in dominant energy regions for the BG distributions at 400 and 1600 K (not shown), respectively. The performance of these schemes were: $n_T=465$ for the current multiple distribution; $n_T=145$ and 140 for $T=15$ and 60 single distributions, respectively. As expected, the efficiency of the current method became clearer when we enlarged the range between U_H and U_L (e.g., $U_L\equiv 0$ nearly corresponds to an average energy of the BG distribution at 300 K), as shown in Table I. We can see that the results for the single distribution depends significantly on the values of U_L and U_H, and that the current method maintains relatively good efficiencies for wide range of the tunneling events.

TABLE I. The number of tunneling events for potential energy trajectory. The event is defined by the events that go from an energy value U_H to a value U_L and back. The trajectories are derived by simulations for single Tsallis distribution with $T=15$, 60 K, and for multiple Tsallis distribution defined from the current scheme.

Range (kcal/mol)		Single distribution		
U_L	U_H	$T=15$ K	$T=60$ K	Multiple distribution
10	130	145	140	465
0	130	133	21	374
10	150	97	122	379

Even so, when an error exists in the simulated values for the sum of distributions, a major reason for the error may come from inaccuracy in the (pre)evaluation of Y^a. Here it is pointed out again that our purpose is not to seek an accurate value of Y^a, but to perform an effective broad sampling of states using a certain designed density. Nevertheless, for practical purposes, it is useful to examine how the results depend on the Y^a value. To do this, we used a fixed value of Y^2 and deviated the Y^1 value from 1; notice that not each value, but only the rate between Y^2 and Y^1 has meaning [multiplications of $Y^1\mapsto c_1Y^1$ and $Y^2\mapsto c_2Y^2$ are equivalent to $Y^1\mapsto(c_1/c_2)Y^1$ and $Y^2\mapsto Y^2$ in the ODE; see Eq. (12) or (21)]. Figure 8 shows the results of the potential energy distributions. As expected, as the Y^1 value increased, the contribution of the (q,ε,T_1) distribution decreased; conversely,

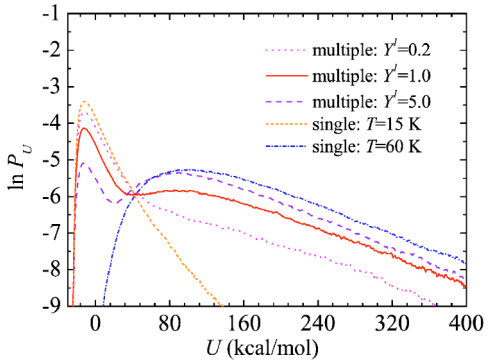

FIG. 8. (Color online) The multi-Tsallis potential-energy distribution density of the alanine system. The partition function rate parameter Y^1 is varied. For comparison, single Tsallis energy distributions at $T=15$ and 60 K are shown.

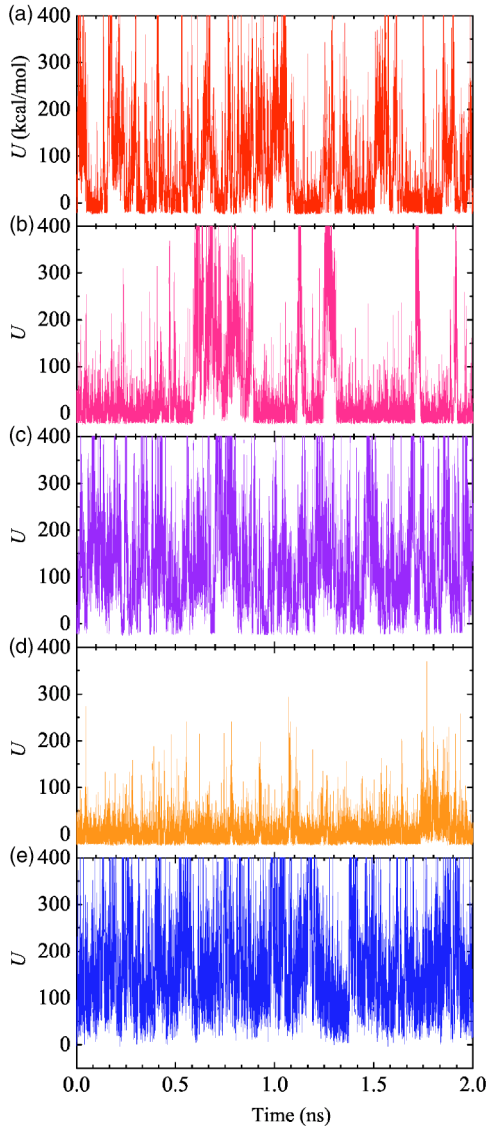

FIG. 9. (Color online) Potential energy trajectories for the alanine system, obtained from the current dynamics for the multi-Tsallis distribution composed of two Tsallis distributions (at $T=15$ and 60 K), where the partition function rate Y^1 was set as 1.0 (a), 0.2 (b), and 5.0 (c). The trajectory obtained from the dynamics for the single Tsallis distribution is shown for $T=15$ K (d) and $T=60$ K (e).

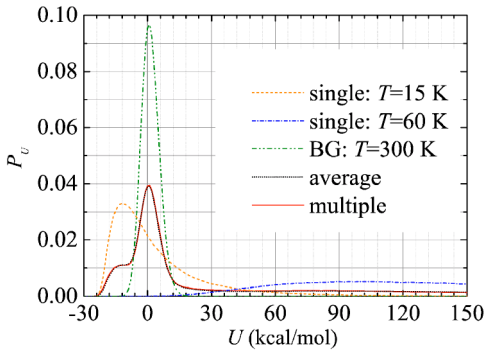

FIG. 10. (Color online) Potential energy distribution density of the alanine system. Dashed, dash-dotted, double-dash-dotted lines are simulated results for the single Tsallis distribution at $T=15$ K and that at 60 K, and the results for the BG distribution at 300 K, respectively. The average of these three single distributions is shown by the dotted line. The corresponding simulated results for the multi-Tsallis distribution combining these three by the current method is shown by the solid line.

that of (q,ε,T_2) distribution increased. It should be noted that in every case, a remarkably wide sampling in the energy space was performed, compared with the case with the BG and Tsallis distributions. Even if an accurate Y^a is not attained, such a broad region sampling, which cannot be easily achieved when only a single distribution is considered, is the most important consequence of this method. The Y^a dependence is discussed also below.

Another characteristic of the current method's results is the natural appearance of the orbit transition among distinct energy regions. Figure 9(a) shows the potential energy trajectory obtained by the current method with $Y^1=1$. Figures 9(b) and 9(c) also show those against the deviated Y^1 values with Y^2 fixed as above. Their behaviors were intrinsically different from those obtained by the dynamics in realizing each single Tsallis distribution, as exhibited in Figs. 9(d) and 9(e) at $T=15$ and 60 K, respectively. The trajectories for the current method consist of two parts: the higher-energy part mainly comes from the contribution of the (q,ε,T_2) distribution, and the lower-energy part from that of (q,ε,T_1). The sojourn time in each part varied with the change in the Y^1 value, in a manner such as that expected from the energy distribution results shown in Fig. 8. In any case, the jump between the two parts, or the (ex)change of the region related to each parameter value, occurred automatically. Since an accurate value of Y^a is not necessarily obtained, this parameter may resemble the uncertain parameter that determines the exchange timing employed in the conventional method with a dynamic view. However, it should be noticed that Y^a has a completely different meaning from that of the uncertain parameter, in that Y^a is not an arbitrarily parameter but has an exact value and thus allows us to use its approximation.

As an extension of our method, we can add more distributions. For example, the BG distribution at 300 K was added to the sum of the above two distributions from the following viewpoint. Suppose that we need information about the energy region corresponding to the 300 K range. Since the targeted region determined from the complicated energy surface is generally disconnected in the phase space, to access a new relevant area will require (i) lower-energy region sampling (to explore) and (ii) higher-energy region sampling (to escape). Thus, as we can see by the example in Fig. 7, this sampling scheme will be performed effectively once we realize the proposed distribution, i.e., the sum of $\overline{\rho^1}$: the Tsallis distribution density with (q,ε,T_1) for (i), $\overline{\rho^2}$: that with (q,ε,T_2) for (ii), and $\overline{\rho^3}$: the added BG distribution density at 300 K (or that with $q_3=1$, any ε_3, and $T_3=300$). As shown in Fig. 4, there is a major overlap between $\overline{\rho^1}$ and $\overline{\rho^2}$ and between $\overline{\rho^1}$ and $\overline{\rho^3}$, so that [putting $c=1$ and permuting $\mathcal{M}=\{1,2,3\}$ by $\sigma=\binom{123}{213}$] we additionally calculated Y^3 using Eq. (27). Figure 10 shows the potential energy distribution densities related to this summation. The results of

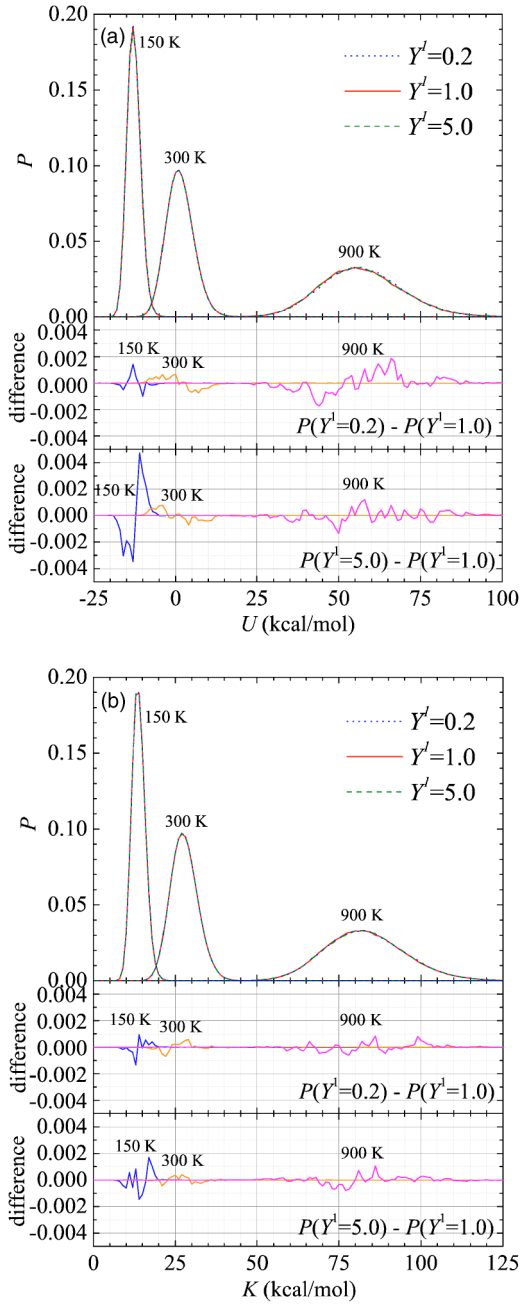

FIG. 11. (Color online) BG energy distribution densities at $T=150$, 300, and 900 K for the alanine system: (a) Reweighted results of potential energy obtained from the simulation realizing multidistribution composed of the Tsallis distribution at 15 K, that at 60 K, and the BG distribution at 300 K, using the indicated Y^1 values (top). The difference of the results for $Y^1=0.2$ (middle) [$Y^1=5.0$ (bottom)] from that for $Y^1=1$. (b) Those for the kinetic energy.

the current method provided, with very good accuracy, the average of the results for the above three distributions otherwise simulated. This demonstrates that these distributions were joined in a quantitatively successful manner again by the current method. We can see that indeed the sampling included both the low-energy region covered by the (q,ε,T_1) distribution and the high-energy region by the (q,ε,T_2) distribution, in addition to the BG energy region. Concerning the Y^a value dependence, we performed simulations using several values of Y^1 corresponding to (q,ε,T_1) also in this case (the major overlap was seen through $\overline{\rho^1}$). In Fig. 11 we show the reweighted results of the BG potential energy distributions at several temperatures as well as the kinetic energy distributions. As shown through the small discrepancies among the distributions for distinct Y^1 values, the results were consistent with each other, indicating that such important physical variable samplings were irrelevant to the exact adjustment of the value of Y^a.

IV. CONCLUSION

We have proposed a deterministic sampling scheme for effectual performance in continuous systems, and we have investigated the fundamental aspects of the scheme in detail. The expectation of a function is given by the average of each expectation for multiple arbitrarily given distributions, which also is the realizing probability for an arbitrary subset in the phase space. This addresses a static feature for realizing multiple distributions and enables us to cover a wide space region. Using the one-dimensional double-well potential model, we have shown that our method works exactly and indeed permits discontinuity of the density of states. Some techniques proposed here have been devoted to sampling well in realistic systems, freeing us from the need for detailed tuning of the parameter value for a targeted single distribution, especially for a Tsallis distribution. A method for constructing a suitable parameter sequence to build an effective multi-Tsallis distribution was proposed by considering the reference temperature and the temperature dependence of the Tsallis distribution. We confirmed these in the alanine tripeptide system. The potential energy trajectories obtained from the current method differed intrinsically from each trajectory derived from a single distribution, but they involved each characteristic. The static feature of the method creates the automatic trajectory jump among the dominant phase-space regions, inducing a nonparametrical scheme with respect to the region exchange. We have also investigated the dependence of simulated issues on the value of the partition function rate, whose adhibition is required, and confirmed the irrelevance of the value to the important physical results. Finally, we have presented the composition method dealing with both the BG distribution, which is targeted as concern, and the Tsallis distributions, which are applied in order to bring a twofold energy bias.

ACKNOWLEDGMENTS

We thank Dr. Yuji Sugita and Dr. Yoshifumi Fukunishi for valuable discussions. The New Energy and Industrial Technology Development Organization is acknowledged for its financial support of this study. We also thank Masaru Horie for help in producing the figures.

[1] F. Faupel, W. Frank, M.-P. Macht, H. Mehrer, V. Naundorf, K. Räzke, H. R. Schober, S. K. Sharma, and H. Teichler, Rev. Mod. Phys. **75**, 237 (2003).

[2] S. Sastry, Nature (London) **409**, 164 (2001).

[3] N. A. Alves and U. H. E. Hansmann, Phys. Rev. Lett. **84**, 1836 (2000).

[4] W. G. Hoover and B. L. Holian, Phys. Lett. A **211**, 253 (1996), and the references therein.

[5] W. G. Hoover, *Computational Statistical Mechanics* (Elsevier, New York, 1991).

[6] Y. Sugita and Y. Okamoto, Chem. Phys. Lett. **314**, 141 (1999).

[7] Y. Sugita, A. Kitao, and Y. Okamoto, J. Chem. Phys. **113**, 6042 (2000).

[8] U. H. E. Hansmann, Y. Okamoto, and F. Eisenmenger, Chem. Phys. Lett. **259**, 321 (1996).

[9] N. Nakajima, H. Nakamura, and A. Kidera, J. Phys. Chem. B **101**, 817 (1997).

[10] S. Jang, Y. Pak, and S. Shin, J. Chem. Phys. **116**, 4782 (2002).

[11] J. G. Kim, Y. Fukunishi, A. Kidera, and H. Nakamura, Phys. Rev. E **68**, 021110 (2003).

[12] A. Mitsutake and Y. Okamoto, J. Chem. Phys. **121**, 2491 (2004), and the references therein.

[13] R. Zhou, B. J. Berne, and R. Germain, Proc. Natl. Acad. Sci. U.S.A. **98**, 14931 (2001).

[14] A. E. Garcia and J. N. Onuchic, Proc. Natl. Acad. Sci. U.S.A. **100**, 13898 (2003).

[15] R. Yamamoto and W. Kob, Phys. Rev. E **61**, 5473 (2000).

[16] K. Ikeda, O. V. Galzitskaya, H. Nakamura, and J. Higo, J. Comput. Chem. **24**, 310 (2003).

[17] N. Nakajima, J. Higo, A. Kidera, and H. Nakamura, Chem. Phys. Lett. **278**, 297 (1997).

[18] Y. S. Watanabe, Y. Fukunishi, and H. Nakamura, J. Mol. Graphics Modell. **23**, 59 (2004).

[19] N. Kamiya, J. Higo, and H. Nakamura, Protein Sci. **11**, 2297 (2002).

[20] S. Ono, N. Nakajima, J. Higo, and H. Nakamura, J. Comput. Chem. **21**, 748 (2000).

[21] C. Tsallis, J. Stat. Phys. **52**, 479 (1988).

[22] C. Tsallis, Braz. J. Phys. **29**, 1 (1999), for an updated bibliography, see http://tsallis.cat.cbpf.br/biblio.htm

[23] I. Andricioaei and J. E. Straub, J. Chem. Phys. **107**, 9117 (1997).

[24] U. H. E. Hansmann, F. Eisenmenger, and Y. Okamoto, Chem. Phys. Lett. **297**, 374 (1998).

[25] Y. Pak and S. Wang, J. Chem. Phys. **111**, 4359 (1999).

[26] A. R. Plastino and C. Anteneodo, Ann. Phys. (N.Y.) **255**, 250 (1997).

[27] I. Fukuda and H. Nakamura, Phys. Rev. E **65**, 026105 (2002).

[28] J. S. Andrade, Jr., M. P. Almeida, A. A. Moreira, and G. A. Farias, Phys. Rev. E **65**, 036121 (2002).

[29] I. Fukuda and H. Nakamura, Chem. Phys. Lett. **382**, 367 (2003).

[30] I. Fukuda and H. Nakamura, J. Phys. Chem. B **108**, 4162 (2004).

[31] A. M. Ferrenberg and R. H. Swendsen, Phys. Rev. Lett. **61**, 2635 (1988).

[32] U. H. E. Hansmann, Phys. Rev. E **56**, 6200 (1997).

[33] T. Terada, Y. Matsuo, and A. Kidera, J. Chem. Phys. **118**, 4306 (2003).

[34] I. Fukuda and H. Nakamura, in *Slow Dynamics in Complex Systems: Third International Symposium on Slow Dynamics in Complex Systems*, edited by Michio Tokuyama and Irwin Oppenheim, AIP Conf. Proc. No. 708 (AIP, Woodbury, 2004), p. 356.

[35] S. Jang, S. Shin, and Y. Pak, Phys. Rev. Lett. **91**, 058305 (2003).

[36] S. Nosé, J. Chem. Phys. **81**, 511 (1984).

[37] W. G. Hoover, Phys. Rev. A **31**, 1695 (1985).

[38] We can also say "ergodicity for ρ [Eq. (10)]," since the ergodicity is an invariant property with respect to a constant multiplication $\hat{s}:\rho\mapsto\tilde{\rho}\equiv s\rho(0<s<\infty)$. So Eq. (15) is concluded directly rather than through Eq. (14). Only change due to $\hat{s}$ is for the invariant measure, as $P\mapsto\tilde{P}\equiv sP$; note that the one-parameter group of automorphism for measure space $(\Gamma,\mathcal{L},P)$ also becomes that for $(\Gamma,\mathcal{L},\tilde{P})$, consistent with the invariance of Eq. (1) with respect to $\hat{s}$, and so the invariance is inherited in Eqs. (8) and (12) [or Eq. (9)].

[39] R. W. Zwanzig, J. Chem. Phys. **22**, 1420 (1954).

[40] J. G. Kirkwood, J. Chem. Phys. **3**, 300 (1935).

[41] N. D. Lu, J. K. Singh, and D. A. Kofke, J. Chem. Phys. **118**, 2977 (2003), and references therein.

[42] For a more accurate and general description about the limit for $|I|\to 0$, refer to, e.g., G. B. Folland, *Real Analysis* (Wiley, New York, 1984), p. 93.

[43] In the present case, from the standpoint of the escort probabilities [44], the form of $b_a\equiv q_a/(1-q_a)$ may not be so useful, since the escort probabilities will lead to a form such as $(\Sigma_{a=1}^{M}\rho^a)^q$ and not $\Sigma_{a=1}^{M}(\rho^a)^{q_a}$; but the form $b_a\equiv q_a/(1-q_a)$ is useful for expediting the finiteness of each partition function, retaining the difference with the BG distribution [30].

[44] C. Tsallis, R. S. Mendes, and A. R. Plastino, Physica A **261**, 534 (1998).

[45] A. R. Plastino and A. Plastino, Phys. Lett. A **193**, 140 (1994).

[46] D. Kusnezov, A. Bulgac, and W. Bauer, Ann. Phys. (N.Y.) **204**, 155 (1990).

[47] I. L'Heureux and I. Hamilton, Phys. Rev. E **47**, 1411 (1993).

[48] S. Nosé, Prog. Theor. Phys. Suppl. **103**, 1 (1991).

[49] A. C. Brańka, M. Kowalik, and K. W. Wojciechowski, J. Chem. Phys. **119**, 1929 (2003).

[50] I. Andricioaei, A. R. Dinner, and M. Karplus, J. Chem. Phys. **118**, 1074 (2003).

[51] B. C. Dian, A. Longarte, and T. S. Zwier, Science **296**, 2369 (2002).

[52] D. J. Tobias, S. F. Sneddon, and C. L. Brooks III, J. Mol. Biol. **216**, 783 (1990).

[53] W. D. Cornell, P. Cieplak, C. I. Bayly, I. R. Gould, K. M. Merz, Jr., D. M. Ferguson, D. C. Spellmeyer, T. Fox, J. W. Caldwell, and P. A. Kollman, J. Am. Chem. Soc. **117** 5179 (1995).

[54] P. Kollman, R. Dixon, W. Cornell, T. Fox, C. Chipot, and A. Pohorille, in *Computer Simulation of Biomolecular Systems*, edited by W. F. van Gunsteren, P. K. Weiner, and A. J. Wilkinson (Kluwer, Netherlands, 1997), Vol. 3, pp. 83–96.

[55] K. Morikami, T. Nakai, A. Kidera, M. Saito, and H. Nakamura, J. Comput. Chem. **16**, 243 (1992).

[56] Y. Fukunishi, Y. Mikami, and H. Nakamura, J. Phys. Chem. B **107**, 13201 (2003).

[57] U. H. E. Hansmann and Y. Okamoto, Phys. Rev. E **56**, 2228 (1997).

[58] This is intuitively obvious. Also in a mathematically rigorous

sense, using elementary facts, the results can be obtained from the assumption that a function f on a closed interval $J \subset \mathbf{R}$ is concave, i.e., $f(\lambda x+(1-\lambda)y) \geqq \lambda f(x)+(1-\lambda)f(y)$ for all $x,y \in J$ and all $\lambda \in (0,1)$: If $f(E_1)=f(E_2)$ holds for inner points $E_1,E_2,(E_1<E_2) \in \mathring{J}$, then a maximum point $E_{\max}$ exists in $[E_1,E_2]$, viz., $f(E_{\max})=\max f(J)$. The assumption for smoothness of f is not needed.

[59] N. D. Lu and D. A. Kofke, J. Chem. Phys. **114**, 7303 (2001).

[60] A. Mitsutake, Y. Sugita, and Y. Okamoto, J. Chem. Phys. **118**, 6664 (2003).